Probing Stress Effects in Single Crystal Organic Transistors by Scanning Kelvin Probe Microscopy

Lucile C. Teague[1], Oana D. Jurchescu[2,3,*], Curt A. Richter[2,] Sankar Subramanian[4], John E. Anthony[4], Thomas N. Jackson[3], David J. Gundlach[2], and James G. Kushmerick[2]

[1]*Savannah River National Laboratory, Aiken, SC 29808*
[2]*National Institute of Standards and Technology, Gaithersburg, Maryland 20899,*
[3]*The Pennsylvania State University, State College, PA 16802*
[4]*Department of Chemistry, University of Kentucky, Lexington, KY 40506*

We report scanning Kelvin probe microscopy (SKPM) of single crystal difluoro bis(triethylsilylethynyl) anthradithiophene (diF-TESADT) organic thin film transistors. SKPM provides a direct measurement of the intrinsic charge transport in the crystals independent of contact effects and reveals that degradation of device performance occurs over a time period of minutes as the diF-TESADT crystal becomes charged.

Scanning Kelvin probe microscopy (SKPM) has demonstrated utility in correlating the relationship between film structure and charge transport in organic thin-film transistor (OTFT) devices as well as providing a detailed view of charge injection at the source and drain contacts.[1-7] While traditional field effect transistor (FET) I-V (performance) measurements yield the average mobility of the device, SKPM offers the advantage of probing the local mobility of the device. Previous studies of rubrene single crystal (SC) OTFTs utilized SKPM data, specifically the slope of the potential profile in the device channel (V/μm), to directly calculate the intrinsic charge mobilities of individual devices (μ).[8] Mobilities calculated as such provide a more direct measurement of the intrinsic charge transport in the organic crystals themselves, and are typically higher than those derived from conventional I-V measurements of FET performance.[3] By nature, conventional I-V measurements yield charge mobility values that are a convolution of several factors including the intrinsic charge mobility of the organic material itself,

* Present Address: Department of Physics, Wake Forest University, Winston-Salem, NC 27109

charge injection effects at the source and drain contacts, and structural variations in the active organic material such as grain boundaries, interface states, defects, etc. Conversely, SKPM measurements provide the opportunity to examine each of these factors independently to understand how each contributes to the overall charge transport behavior in an organic-based device.

To date, these studies have been motivated by the demand for high performance, low power, and low-cost device structures that can be utilized for a wide range of applications. With that, there is significant interest in comparing the structural and electronic properties of OTFT devices made from different manufacturing and deposition/processing methods as well as from different organic materials. The material studied here, difluoro bis(triethylsilylethynyl) anthradithiophene (diF-TESADT), is one of a number of "designer" organic materials being studied for potential use in organic based electronics.[9] Charge mobilities on the order of 0.4 $cm^2/V•s$ have been achieved for diF-TESADT spun-cast devices,[10] while charge mobilities of 6 $cm^2/V•s$ have been achieved for single crystal (SC) diF-TESADT OTFTs.[11]

Previous studies of spun-cast OTFTs using other organic materials have reported stress effects such as a decrease in drain current and a shift in the threshold voltage (V_T) when the organic material is under an applied gate bias over a period of several hours and these bias stress effects in the linear vs. saturation regimes have been compared.[12] More recent studies report regions of trapped charge in spun-cast diF-TESADT OTFT devices once the applied gate bias is removed.[13] The results presented herein differ from those referenced above in that they reveal localized intrinsic changes in charge injection and transport over the timescale of *several minutes* for single crystal devices. SKPM was

used to obtain spatially resolved surface potential maps of SC diF-TESADT OTFTs *during* operation in the saturation regime (V_{DS} = -10 V and V_{GS} = -40 V). From these data we were able to directly calculate the intrinsic charge transport of the organic material, to examine the charge injection effects at the source and drain, and to investigate the effect of bias-stress on the electrical properties.

The synthesis of diF-TESADT and subsequent growth conditions for diF-TESADT single crystals have been previously reported.[11, 14] For SKPM studies, single crystals were laminated onto ultraviolet ozone cleaned, thermally oxidized heavily doped Si(100) substrates treated with octyltrichlorosilane (OTS) as described elsewhere.[11] Ti/Au (≈5 and ≈ 40 nm, respectively) source and drain contacts were patterned onto the SiO_2 by e-beam evaporation and patterned by photolithography and a lift-off process.

Initial testing of SC transistor performance was done using an Agilent 4155C semiconductor parameter analyzer[15] while topographic and surface potential data for the SC device structures was obtained under ambient conditions with a XE100 atomic force microscope (AFM) (Park Systems, Santa Clara, CA, USA) as described previously.[7] Drain–source voltages (V_{DS}) and gate voltages (V_{GS}) were applied to the devices (mounted in a ceramic DIP) with a HP 4145B semiconductor parameter analyzer. Additionally, the transistor transport characteristics were measured for each device as wired in the AFM, immediately before and after SKPM scanning for each crystal.

In general, SKPM of SC diF-TES-ADT devices revealed potential drops at the contact edge ranging from ≈ 1.5 V to 5 V in the saturation region (V_{DS} = -10 V and V_{GS} = -40 V). Although a number of devices were investigated, we focus on the results of two specific devices herein that are representative of those studied. The external charge

mobilities (saturation regime) calculated from traditional I-V measurements for these two devices were 3.22 $cm^2/V•s$ (device 80N, Figure 1) and 2.75 $cm^2/V•s$ (device 100K, supporting information). In contrast, we report the intrinsic charge mobilities from SKPM measurements which do not include the contact effects but rather are calculated based on the slope of the potential drop in the channel (V/μm) and the recorded I_{DS}. Specifically, the intrinsic charge mobilities calculated for the diF-TESADT crystals discussed herein ranged from ≈ 2.4 $cm^2/V•s$ (80N) and ≈ 5.5 $cm^2/V•s$ (100K) at the start of the SKPM scan to ≈ 0.6 $cm^2/V•s$ (80N) and ≈ 1.6 $cm^2/V•s$ (100K) at the end of the SKPM scan. Line scans taken at the beginning, middle, and end of the SKPM scan (Figure 2, device 80N) reveal that the slope of potential drop in the device channel remains relatively constant while changes in charge injection behavior at the contacts are observed. These data suggest that because the drop in the potential is relatively constant over the time of the scan, the difference in the calculated intrinsic mobilities is a result of the variation in current (I_{DS}) over the time of the scan resulting from charging of the crystal, which is indicated by the observed changes in the charge injection at the contacts. We discuss these results in detail below. We also note that transport measurements taken for each device as wired in the AFM, before and after SKPM scanning indicate some degradation of device performance.[16] This change is most likely a stress effect due to

repeated operation of the device in the "ON" state for 5 or more minutes at the time.

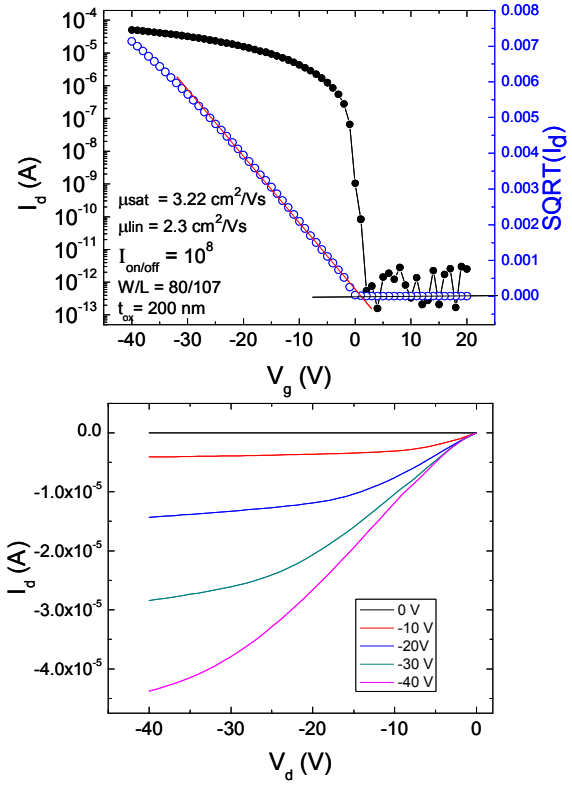

FIG 1. Transfer and transport characteristics of diF-TESADT single crystal FET device labeled 80N in this study (channel length 80 μm, channel width 107 μm).

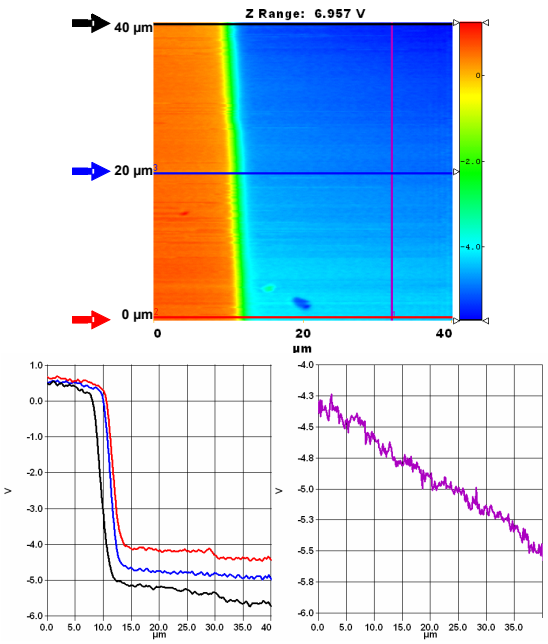

FIG. 2. (Color) SKPM potential image and line profiles for device 80N. Red, blue and black arrows indicate positions of line profiles in X (fast scan direction) shown for beginning, middle, and end of collected image, respectively. The vertical purple line indicates location of line profile in the slow-scan direction (Y). Line profiles indicate a change in the charge injection at the contact occurs over time as the device remains in the "ON" state, with little variation observed in the slope of the potential drop in the device channel (intrinsic charge mobility). The observed slope in slow scan direction is directly proportional to the change in the charge injection barrier over the timescale of the scan.

These observed changes in charge injection over time reveal possible stress effects or charging effects in the crystal as the device is left in the "ON" state for an extended period of time. During data collection, we repeatedly noted an asymptotic decrease in I_{DS} over the duration of the scan, with the largest changes in I_{DS} observed within the first 2-3 minutes of operation in the "ON" state. The initial and final I_{DS} values were recorded and were used to calculate the initial and final charge mobilities from SKPM line scans. In some cases, we allowed the source–drain current to reach a steadier state, waiting ≈ 2-3 mins after applying V_{DS} and V_{GS} before starting the SKPM scan. Line profiles in the X

(fast) scan direction shown in Figure 2 reveal a variation in the potential drop at the contacts indicating a change in charge injection or contact resistance as a function of time while the slope of the potential drop in the device channel (charge mobility) remains fairly constant. It is interesting to note that the change in the potential drop at the Au contact is directly proportional to the change in potential observed in the Y direction; i.e. in device 80N the potential drop at the contact changes ≈ 1 V from the beginning of the scan to the end of the scan while the change in the Y direction is ≈ 1.1 V. These results suggest that the active organic material can become charged over a timescale of a few minutes, decreasing the current flow in the device from source to drain. As the organic material becomes charged, the capacity to inject more holes into the device is reduced, thus increasing the observed potential drop at the contacts. This charge trapping may be a result of layer-to-layer charge transport within the organic material.

SKPM data taken at the drain contacts are consistent with these conclusions. The observed changes in both the charge injection barrier at the drain and the slope of the potential profile in the Y scan direction within the device channel are both inversely proportional to those reported at the source contact.[17] Overall, this inverse relationship indicates a conservation of charge within the device and supports the idea that the organic crystal becomes charged over time.

Recent work by Mahron et al.[13], utilized high-vacuum electric force microscopy (EFM) to examine the distribution and lifetime of trapped charges in spun-cast diF-TESADT devices following the application of a negative gate bias. We find that our results for the SC diF-TESADT devices presented here are in general agreement with recent studies by Mahron and co-workers in that we both observe the presence of trapped

charge in diF-TESADT devices. In contrast to their studies, we examine the changes in the device *during* the application of V_{DS} and V_{GS}, rather than after application of V_{GS}. In our studies, the application of constant bias throughout the measurement yields a continuous supply of free carriers into the organic crystal, while the observed change in the charge injection barrier at the contacts reveals that, over time, some of these mobile charges are converted into trapped charge. This accumulation of charge is observed when the bias is removed from the crystal and the device is turned "OFF" (Figure 3). If we assume a planar density of injected holes, $h_i = C_i(V_G - V_T)$ where C_i is the gate capacitance per unit area and V_T is the threshold voltage[13] proportional to the charge injection barrier at the contact, we can begin to estimate the rate of trap formation/filling over the time of the SKPM scan. Based on these assumptions (with C_i and V_G constant), we estimate the rate of trap formation/filling to be $\approx 4.3 \times 10^{-3}$ V/s over the time of the SKPM scan. We repeatedly observed dissipation of this trapped charge within several minutes of the device being turned "OFF".

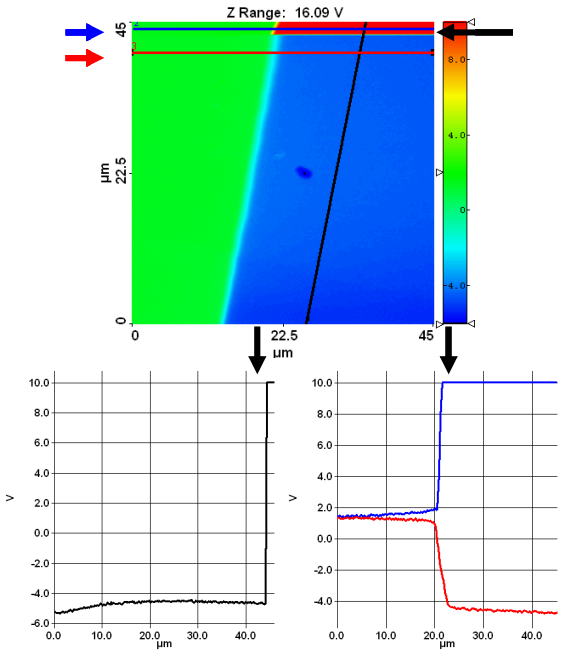

FIG. 3. (Color) SKPM potential image and line profiles for device 80N. Red and blue arrows to the left of the SKPM image indicate positions of line profiles in X shown for crystal in "ON" and "OFF" state, respectively (black arrows indicate switching point in all three plots). The vertical black line indicates location of line profile in the Y approximately 10μm from contact edge. The observed slope in Y when the device is in the "ON"state is due to charging of the crystal. Once the device is turned "OFF", the large change in potential observed indicates that the crystal is becoming positively charged. This effect is most easily observed by comparing the two line profiles in the X direction (red and blue).

The combination of electrical transport and SKPM data presented here reveal that the performance of OTFT devices can be susceptible to stress effects/charging due to operation in the "ON" state over timescales *as short as a few minutes*. SKPM measurements of the localized intrinsic changes in charge injection and transport for these operational SC OTFT devices reveal that the changes in performance are most likely due to an accumulation of charges within the crystal. Furthermore, from these data we were able to provide an estimate of the rate of trap formation/filling required to yield the observed results.

LCT gratefully acknowledges financial support under the SRNL LDRD program. This document was prepared in conjunction with work accomplished under Contract No. DE-AC09-08SR22470 with the U.S. Department of Energy.

References:

1. K. P. Puntambekar, P. V. Pesavento and C. D. Frisbie, Appl. Phys. Lett. **83** (26), 5539-5541 (2003).
2. J. A. Nichols, D. J. Gundlach and T. N. Jackson, Appl. Phys. Lett. **83** (12), 2366-2368 (2003).
3. L. Bürgi, H. Sirringhaus and R. H. Friend, Appl. Phys. Lett. **80** (16), 2913-2915 (2002).
4. L. Bürgi, T. J. Richards, R. H. Friend and H. Sirringhaus, J. Appl. Phys. **94**, 6129-6137. (2003).
5. L. Chen, R. Ludeke, X. Cui, A. G. Schrott, C. R. Kagan and L. E. Brus, J. Phys. Chem. B **109**, 1834-1838 (2005).
6. Y. Luo, F. Gustavo, J.-Y. Henry, F. Mathevet, F. Lefloch, M. Sanquer, P. Rannou and B. Grevin, Advanced Materials **19**, 2267-2273 (2007).
7. L. C. Teague, B. H. Hamadani, O. D. Jurchescu, S. Subramanian, J. E. Anthony, T. N. Jackson, C. A. Richter, D. J. Gundlach and J. G. Kushmerick, Advanced Materials **20**, 4513-4516 (2008).
8. Y. Luo, F. Gustavo, J. Y. Henry, F. Mathevet, F. Lefloch, M. Sanquer, P. Rannou and B. Grevin, Advanced Materials **19** (17), 2267-+ (2007).
9. D. J. Gundlach, J. E. Royer, S. K. Park, S. Subramanian, O. D. Jurchescu, B. H. Hamadani, A. J. Moad, R. J. Kline, L. C. Teague, O. Kirillov, C. A. Richter, J. G. Kushmerick, L. J. Richter, S. R. Parkin, T. N. Jackson and J. E. Anthony, Nature Materials **7**, 216-221 (2008).

10. O. D. Jurchescu, B. H. Hamadani, H. D. Xiong, S. K. Park, S. Subramanian, N. M. Zimmerman, J. E. Anthony, T. N. Jackson and D. J. Gundlach, Appl. Phys. Lett. **92**, 132103 (2008).
11. O. D. Jurchescu, S. Subramanian, R. J. Kline, S. D. Hudson, J. E. Anthony, T. N. Jackson and D. J. Gundlach, Chemistry of Materials **20**, 6733-6737 (2008).
12. S. G. J. Mathijssen, M. Colle, A. J. G. Mank, M. Kemerink, P. A. Bobbert and D. M. de Leeuw, Appl. Phys. Lett. **90** (19), 3 (2007).
13. M. J. Jaquith, J. E. Anthony and J. A. Marohn, J. Mater. Chem. **19**, 6116-6123 (2009).
14. S. Subramanian, S. K. Park, S. R. Parkin, V. Podzorov, T. N. Jackson and J. E. Anthony, J. Am. Chem. Soc. **130**, 2706-2707 (2008).
15. NIST Disclaimer: Certain commercial equipment, or materials are identified in this paper to foster understanding. Such identification does not imply recommendation or endorsement by the National Institute of Standards and Technology, nor does it imply that the materials or equipment identified are necessarily the best available for this purpose.
16. See supplementary material for transport measurements before and after repeated operation in the "ON" state.
17. See supplementary material for SKPM measurements of device 100K.

Supplemental Information:

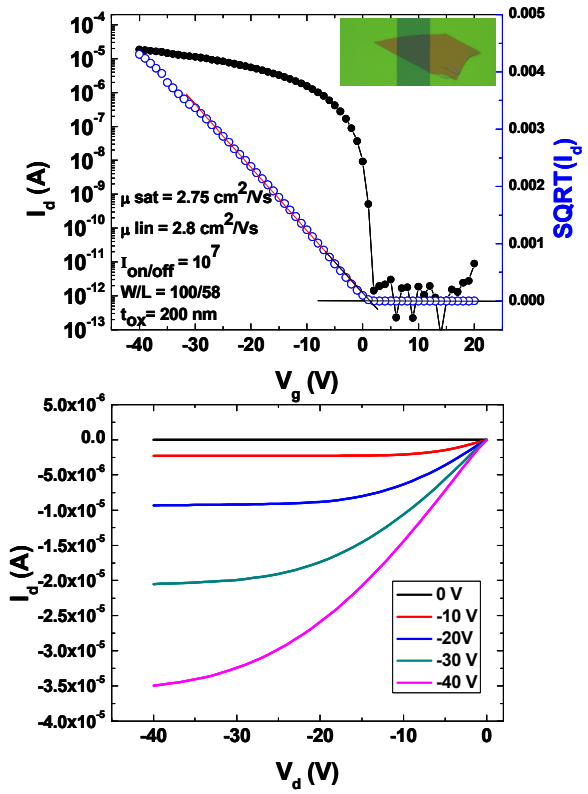

Electrical characteristics of device 100K.

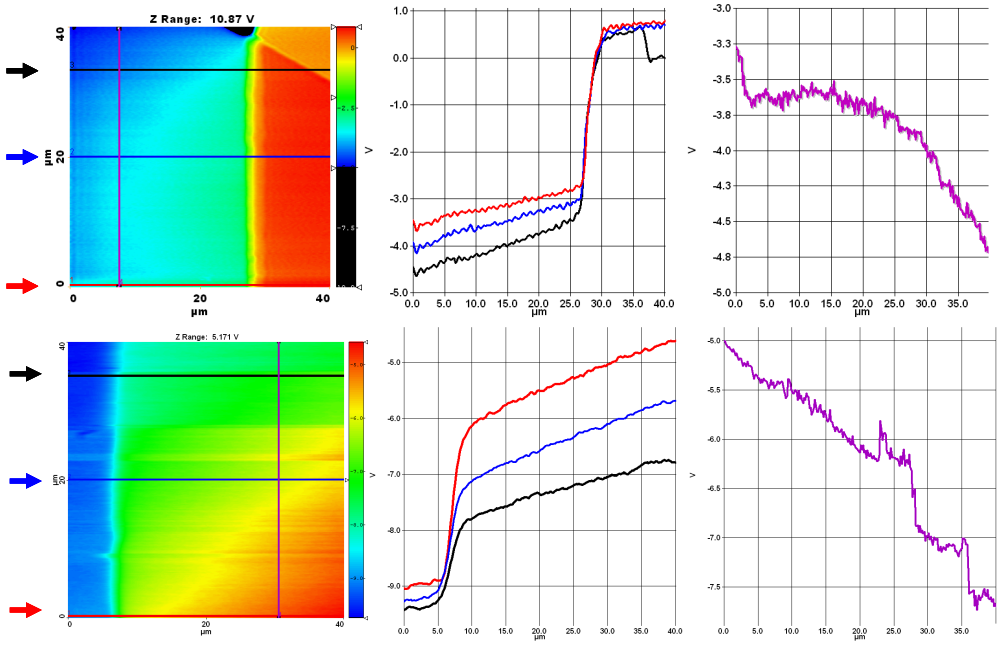

SKPM potential images and line profiles at the source (top) and drain (bottom) contacts for device 100K. Arrows to the left of the images indicate positions of line profiles in X (fast scan direction) shown for beginning, middle, and end of collected image. Vertical lines indicate position of line profile in Y (slow scan direction).

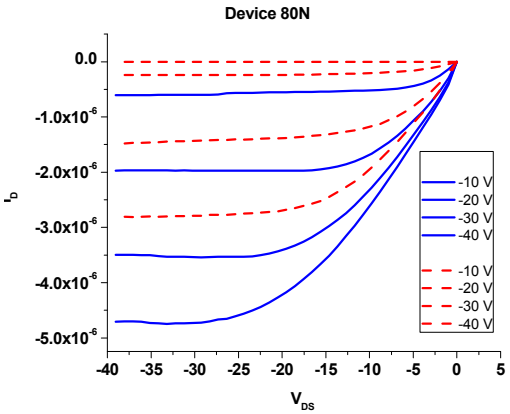

Transport characteristics of device 80N in SKPM setup before (solid lines) and after (dashed lines) repeated operation in the "ON" state at V_{DS} = -10 V and V_{GS} = -40 V (during SKPM measurements).